The EMBO Journal (2012) 31, 2839–2851 | © 2012 European Molecular Biology Organization | Some Rights Reserved 0261-4189/12
www.embojournal.org

THE EMBO JOURNAL

EMBO open

Oncogene-induced telomere dysfunction enforces cellular senescence in human cancer precursor lesions

Anitha Suram[1], Jessica Kaplunov[2], Priyanka L Patel[1], Haihe Ruan[1], Aurora Cerutti[3], Virginia Boccardi[1], Marzia Fumagalli[3,7], Raffaella Di Micco[3,8], Neena Mirani[4], Resham Lal Gurung[5], Manoor Prakash Hande[5], Fabrizio d'Adda di Fagagna[3,6] and Utz Herbig[1,2,*]

[1]New Jersey Medical School-University Hospital Cancer Center, UMDNJ-New Jersey Medical School, Newark, NJ, USA, [2]Department of Microbiology and Molecular Genetics, UMDNJ-New Jersey Medical School, Newark, NJ, USA, [3]IFOM Foundation—FIRC Institute of Molecular Oncology Foundation, Milan, Italy, [4]Department of Pathology and Laboratory Medicine, UMDNJ-New Jersey Medical School, Newark, NJ, USA, [5]Department of Physiology, Yong Loo Lin School of Medicine, National University of Singapore, Singapore and [6]Istituto di Genetica Molecolare, Consiglio Nazionale delle Ricerche, Pavia, Italy

In normal human somatic cells, telomere dysfunction causes cellular senescence, a stable proliferative arrest with tumour suppressing properties. Whether telomere dysfunction-induced senescence (TDIS) suppresses cancer growth in humans, however, is unknown. Here, we demonstrate that multiple and distinct human cancer precursor lesions, but not corresponding malignant cancers, are comprised of cells that display hallmarks of TDIS. Furthermore, we demonstrate that oncogenic signalling, frequently associated with initiating cancer growth in humans, dramatically affected telomere structure and function by causing telomeric replication stress, rapid and stochastic telomere attrition, and consequently telomere dysfunction in cells that lack hTERT activity. DNA replication stress induced by drugs also resulted in telomere dysfunction and cellular senescence in normal human cells, demonstrating that telomeric repeats indeed are hypersensitive to DNA replication stress. Our data reveal that TDIS, accelerated by oncogene-induced DNA replication stress, is a biological response of cells in human cancer precursor lesions and provide strong evidence that TDIS is a critical tumour suppressing mechanism in humans.

The EMBO Journal (2012) **31,** 2839–2851. doi:10.1038/emboj.2012.132; Published online 8 May 2012
Subject Categories: signal transduction; molecular biology of disease
Keywords: cancer progression; cellular senescence; oncogene; telomere dysfunction; tumour suppressing mechanism

*Corresponding author. Department of Microbiology and Molecular Genetics, New Jersey Medical School-UH Cancer Center, UMDNJ, CC-G1226, 205 South Orange Avenue, Newark, NJ 07103, USA.
Tel.: +1 973 972 4426; Fax: +1 973 972 1875;
E-mail: herbigut@umdnj.edu
[7]Current address: TTFactor Srl, Milan, Italy
[8]Current address: Department of Pathology, New York University School of Medicine, New York, NY, USA

Received: 14 October 2011; accepted: 16 April 2012; published online: 8 May 2012

Introduction

Dysfunctional telomeres play a critical role in the progression of human cancer. In the context of deregulated DNA damage checkpoint signalling, telomere dysfunction can promote cancer progression by seeding the events that lead to chromosomal instability. This situation is observed in advanced cancer precursor lesions such as ductal carcinoma *in situ* (DCIS) (Chin *et al*, 2004) and colonic adenomas with high-grade dysplasia (Rudolph *et al*, 2001). When DNA damage checkpoint responses are intact, however, telomere dysfunction leads to cellular senescence, a permanent and stable proliferative arrest that functions as a cell intrinsic tumour suppressing mechanism in mouse model systems (Sharpless and DePinho, 2005; Cosme-Blanco *et al*, 2007; Feldser and Greider, 2007). Cells with dysfunctional telomeres have been detected in cancers with low mitotic activity, such as early stage B-cell chronic lymphocytic leukaemia, suggesting that telomere dysfunction also poses a barrier to cancer progression in humans (Augereau *et al*, 2011). However, direct evidence that telomere dysfunction-induced cellular senescence (TDIS) is an *in vivo* physiologic response that limits progression of human cancer is still missing.

Cellular senescence is thought to limit cancer progression by preventing the proliferation of cells in early neoplastic lesions. Studies conducted using mouse model systems suggest that cellular senescence arrests tumour growth before cells become malignant and invade surrounding tissue (Collado and Serrano, 2010). Similarly, cells with senescence-like features have also been detected in benign human cancer precursor lesions, but are absent in malignant cancers, supporting the conclusions that this stable growth arrest limits cancer progression at premalignant stages. In mouse models, the tumour suppressing functions of cellular senescence can be triggered by oncogenes (Braig *et al*, 2005; Collado *et al*, 2005; Michaloglou *et al*, 2005), loss of growth regulatory mechanisms (Chen *et al*, 2005), or dysfunction of telomeres (Cosme-Blanco *et al*, 2007; Feldser and Greider, 2007), but the mechanisms ultimately triggering cellular senescence in human cancer precursor lesions are still incompletely understood.

Entry into senescence is regulated by at least two signalling pathways: a stress-induced $p16^{INK4a}$/Rb-dependent pathway and a DNA damage response (DDR) pathway that is mediated by p53 (Herbig and Sedivy, 2006). While the molecular activators of the $p16^{INK4a}$/Rb pathway are largely unknown, p53 is activated primarily in response to DNA damage such as double-stranded DNA breaks (DSBs). In human cell cultures, a primary reason for senescence is because telomeres progressively shorten with every cell cycle until a critical length is reached that causes telomeres to become dysfunctional. Telomere erosion is a consequence of a variety of factors that include the inability of the replicative

polymerase to completely duplicate linear DNA (also called 'end replication problem'), postreplicative processing of chromosome ends, and sporadic telomere attrition due to repair events at damaged telomeres (Lansdorp, 2005). Once telomeres become dysfunctional, they are sensed as DSBs and consequently activate the DDR/p53 senescence pathway (d'Adda di Fagagna *et al*, 2003; Takai *et al*, 2003; Herbig *et al*, 2004).

Cellular senescence can also be induced prematurely before telomere shortening due to continuous cell proliferation becomes growth limiting. Dysregulated oncogenes, for example, cause cells to undergo oncogene-induced senescence (OIS) after a brief period of hyperproliferation. Depending on cell type, signal strength, and extracellular environment, oncogenes activate distinct and sometimes complex signalling networks that likely each contribute to various degrees to the permanent growth arrest that characterizes OIS (Courtois-Cox *et al*, 2008). Oncogenic signals also cause high levels of DNA replication stress, which leads to the formation of DSBs and activation of a persistent DDR (Bartkova *et al*, 2006; Di Micco *et al*, 2006). Since aberrant oncogene signalling frequently initiates cancer growth in humans (Hanahan and Weinberg, 2011), and signs of a persistent DDR are observed in several benign and malignant human neoplasms (Bartkova *et al*, 2005, 2007; Gorgoulis *et al*, 2005; Nuciforo *et al*, 2007), it is currently thought that the reasons for the inactive nature of human cancer precursor lesions is because cells within these lesions had undergone OIS. Here, we further characterize the causes for cellular senescence in cancer precursor lesions and provide compelling evidence that telomeres play a critical role in preventing malignant cancer progression in humans.

Results

Human nevi are comprised of cells that display hallmarks of TDIS

Cells displaying senescence-like features such as senescence-associated β-galactosidase activity, elevated levels of p16, and signs of an activated DDR, have been detected in human nevi, suggesting that cellular senescence limits melanoma progression at premalignant stages (Gorgoulis *et al*, 2005; Michaloglou *et al*, 2005; Gray-Schopfer *et al*, 2006). To characterize specifically which senescence pathway was activated in cells of human nevi, we immunostained benign and dysplastic nevi (Supplementary Figure S1A) for p16 and for 53BP1, a cytological marker of DDR activation (Adams and Carpenter, 2006). In agreement with previous studies (Michaloglou *et al*, 2005; Gray-Schopfer *et al*, 2006), we detected heterogeneous p16 levels and a mosaic p16 expression pattern in cells of nevi (Supplementary Figure S1B and C). These data therefore suggest that the p16/Rb senescence pathway alone is not responsible for arresting melanocytic cells at this stage of cancer development. In contrast, the great majority (~90%) of cells within 26 analysed nevi displayed discrete 53BP1 foci, independent of patient age, demonstrating a massive activation of a DDR in premalignant melanocytic lesions (Figure 1A and B; Supplementary Figure S1C and E). The majority of normal melanocytes in the dermal–epidermal junction of analysed samples lacked 53BP1 foci, demonstrating that 53BP1 focus formation is not an intrinsic property of melanocytes in tissue (Figure 1B; Supplementary Figure S1D and E). Interestingly, we observed an ageing-associated increase of 53BP1-positive normal melanocytes in the epidermis of these patients, suggesting that the observed heterogeneity in 53BP1-positive normal cells was attributed to patient age (Supplementary Figure S1E). Similar to normal melanocytes, cells of invasive melanoma showed infrequent and heterogeneous staining for 53BP1 foci. Vertical growth phase melanomas and melanocytic cells in deep soft tissue generally lacked signs of a DDR, while cells in radial growth phase melanoma often displayed discrete 53BP1 foci, albeit at a lower frequency compared with cells in nevi (Figure 1A and B; Supplementary Figure S1F). These observations are consistent with the reported down-regulation of DDR activity in more advanced human cancers (Bartkova *et al*, 2005, 2007; Gorgoulis *et al*, 2005; Nuciforo *et al*, 2007). Together, our data demonstrate a substantial and consistent accumulation of DDR-positive melanocytes in nevi, but not in the epidermis or in malignant melanomas.

In replicative senescent human cells, persistent DDR foci are frequently associated with short and dysfunctional telomeres (d'Adda di Fagagna *et al*, 2003; Herbig *et al*, 2004). To test whether the DDR was a consequence of telomere dysfunction, we analysed tumour tissue for the presence of telomere dysfunction-induced DNA damage foci (TIF), or colocalizations between telomeres, labelled using a telomeric peptide nucleic acid (PNA), and DDR foci as we have done previously (Herbig *et al*, 2004). Images were acquired at high magnification ($\times 100$) and in *z*-series throughout the entire thickness of the tissue using a fluorescence microscope equipped with an ApoTome. This generated images of consecutive 0.3–0.4 μm optical slices and therefore minimized any coincidental overlap between two distinct foci along the optical *z*-axis (Supplementary Figure S2A and B). Using this technique, we discovered that over 60% of all DDR foci analysed in nevi colocalized with telomeric repeats (Figure 1C; Supplementary Figure S2C). Similarly, the few remaining DDR foci in cells of melanoma were also primarily telomeric, albeit to a lesser degree compared with 53BP1 foci in nevi (Supplementary Figure S2C). In contrast, only 6% of DDR foci colocalized with centromeric foci, visualized using antibodies against centromeric proteins, supporting our conclusions that the DDR was specific to telomeres (Supplementary Figure S2D). Of note, the few colocalizations between centromeric signals and DDR foci also demonstrates that our imaging technique is sensitive enough to discriminate coincidental overlap between two random foci within a cell nucleus. Dysfunctional telomeres in cells of nevi retained the shelterin component TRF2, arguing against the possibility that telomere dysfunction in these cells was a consequence of TRF2 loss and/or degradation (Supplementary Figure S2E).

In order to quantitate the percentages of cells containing dysfunctional telomeres in tissue, we scored cells as TIF positive when 50% of 53BP1 foci in a cell nucleus colocalized with telomeric repeats. We discovered that the majority of melanocytic cells in benign (64%) and dysplastic nevi (70%) were indeed TIF positive, which was in contrast to cells in malignant melanoma that infrequently scored as TIF positive (11%; Figure 1D). Thus, despite the apparent lack of total telomere shortening in melanocytic cells of human nevi (Michaloglou *et al*, 2005), the data presented here suggest that cells within these lesions had undergone TDIS.

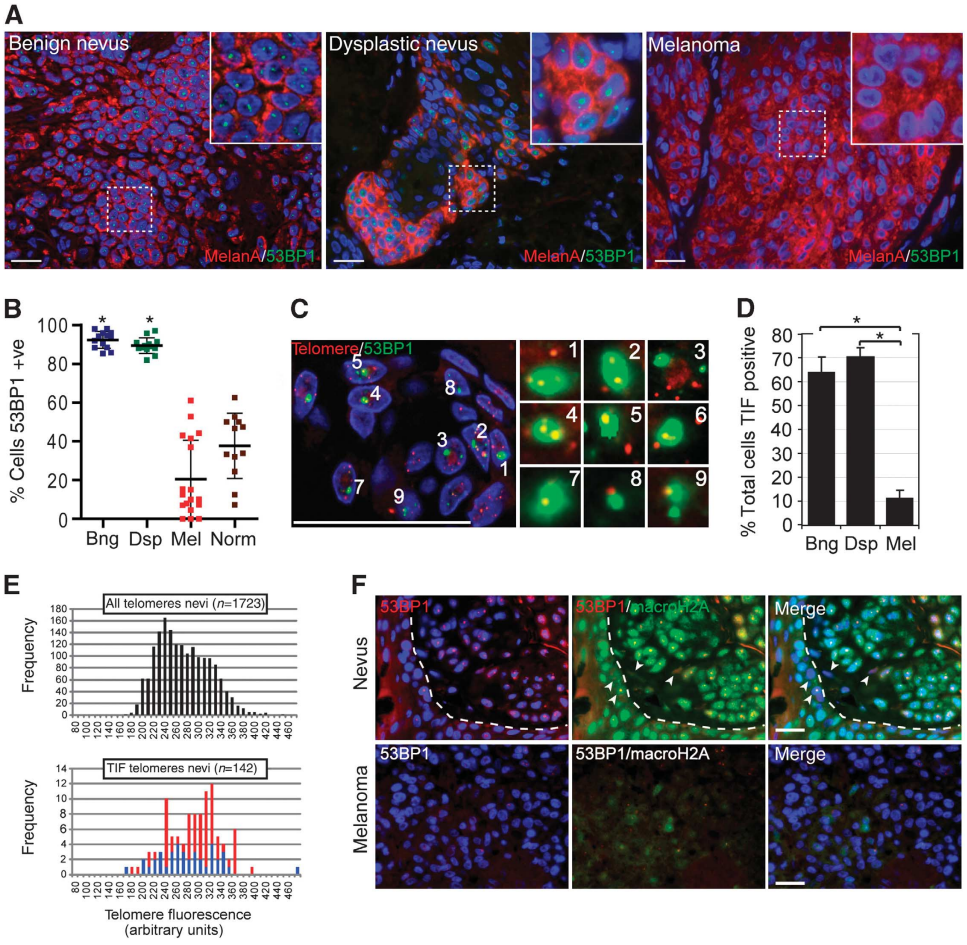

Figure 1 Melanocytic cells of benign- and dysplastic nevi, but not cells of malignant melanoma, display hallmarks of telomere dysfunction-induced cellular senescence. (**A**) Tissue sections from indicated lesions were immunostained with antibodies against melanA (red) and 53BP1 (green). Insets display an enlarged section of the indicated area. (**B**) Quantitation of 53BP1-positive melanocytic cells in benign nevi (Bng; $n=13$, 3529 cells), dysplastic nevi (Dsp; $n=13$, 2300 cells), melanoma (Mel; $n=18$, 5401 cells), and in normal epidermal melanocytes adjacent to the lesion (Norm; $n=12$, 485 cells). Values are shown as mean ± s.d.; $^*P<0.001$. (**C**) Dysfunctional telomeres in nevi. Tissue sections from benign nevi were processed by immunoFISH to simultaneously detect 53BP1 (green) and telomeres (red). Enlarged versions of the numbered DNA damage foci showing colocalization with telomeres are shown in the right micrographs. Note that only one optical slice is displayed. (**D**) Quantitation of TIF positive cells in indicated lesions (mean ± s.d.). A total of 13 benign nevi (1355 53BP1 foci), 13 dysplastic nevi (2968 53BP1 foci), and 7 melanoma (891 53BP1 foci) were counted; $^*P<0.001$. (**E**) Distribution of telomere lengths based on their signal intensities (*x*-axis; arbitrary units). Top histogram: all telomeric signals in cells of nevi (average signal intensity 268 ± 46). Bottom histogram: single (red bars; average signal intensity 281 ± 46) and multiple/diffuse (blue bars; average signal intensity 275 ± 56) telomeric signals associated with 53BP1 foci. *n*: number of telomeric signals analysed (**F**) Tissue sections from a dysplastic naevus (top), and invasive melanoma (bottom) were immunostained using antibodies against 53PB1 (red) and macroH2A (green). Arrows point to stromal cells and basal layer epidermal keratinocytes that did not display elevated macroH2A levels. Dashed line separates epidermis (bottom left) from naevus (top right). Scale bars: 25 μm. Statistical significance was calculated by one-way ANOVA followed by Tukey's *post hoc* test.

Although it has been reported that total telomere lengths in cells of nevi are similar to those of surrounding stromal cells, it is possible that the DDR in melanocytic cells was initiated by one or few telomeres that had become critically short and dysfunctional due to stochastic telomere attrition events (Michaloglou *et al*, 2005). To test this possibility, we quantified fluorescence signal intensities of telomeres in TIF (Figure 1E, red and blue bars) and compared these with signal intensities of telomeres not associated with DDR foci (Figure 1E, black bars). Surprisingly, our analysis revealed that telomeric foci colocalizing with 53BP1 (Figure 1E, red bars) emitted on average similar fluorescence signal intensities compared with the other telomeres in the same cells (Figure 1E, black bars), suggesting that telomere dysfunction in these cells was not primarily due to critical telomere attrition. We also discovered that ~30% of all dysfunctional telomeres analysed displayed telomeric doublets or diffuse telomere signals, suggesting that these structures were either fragile telomeres (Sfeir *et al*, 2009) or alternatively, aggregation of multiple dysfunctional telomeres within one DDR focus as described recently in senescent human fibroblast cultures (Figure 1C and E; Supplementary Figure S2F) (Kaul *et al*, 2011). To distinguish between these two possibilities, we measured the combined fluorescence intensities of telomeric doublets in DDR foci and discovered that these combined values (Figure 1C, blue bars) were similar to intensity values of individual telomere signals in DDR foci. Given that DDR-associated telomeric aggregates

almost always display greater combined fluorescence signal intensities compared with the other telomeres in the same cells (Kaul *et al*, 2011), it is unlikely that these aberrant telomeric structures are due to aggregation of multiple dysfunctional telomeres in a single DDR focus.

Elevated levels of some heterochromatin proteins are a feature of senescent melanocytes in culture (Michaloglou *et al*, 2005; Bandyopadhyay *et al*, 2007) and have been used as a marker to detect senescent cells in tissue (Collado *et al*, 2005; Herbig *et al*, 2006; Jeyapalan *et al*, 2007; Majumder *et al*, 2008). Using antibodies against macroH2A, a late-appearing molecular component of senescence-associated heterochromatin (Zhang *et al*, 2005) and a suppressor of melanoma progression (Kapoor *et al*, 2010), we observed that virtually all melanocytic cells in analysed nevi displayed elevated macroH2A levels (Figure 1F). Similar observations have also been reported recently (Kapoor *et al*, 2010). Together with studies demonstrating senescence-associated β-galactosidase activity in nevi (Michaloglou *et al*, 2005; Gray-Schopfer *et al*, 2006), our observations not only support previous conclusions that cells in nevi are senescent, but also strongly suggest that elevated levels of macroH2A are a feature specific to senescent cells *in vivo*. In support of this, we show that nuclear staining of the cell proliferation marker Ki67 and of macroH2A was mutually exclusive in early invasive melanocytic lesions that display features of both senescence and proliferation (Supplementary Figure S3A). In contrast to cells of nevi, few normal epidermal melanocytes displayed elevated macroH2A levels (Supplementary Figure S3B). Similarly, macroH2A levels in cells of melanomas in deep soft tissue were generally low, suggesting that cells of these invasive cancers had either lost the ability to undergo senescence or did not encounter signals leading to cellular senescence (Figure 1F). In nevi, cells that stained positive for 53BP1 also displayed elevated levels of macroH2A, revealing a positive correlation between DDR activation and the senescence status (Figure 1F). No correlation between telomere dysfunction and p16 upregulation could be established (Supplementary Figure S1C).

Breast- and colon-cancer precursor lesions display hallmarks of TDIS

Our data are consistent with the idea that TDIS limits melanoma progression at premalignant stages. To determine whether the potential tumour suppressing functions of TDIS are limited to melanocytic cells of nevi or also affect the growth of epithelial tumour cells, we analysed colonic (tubular) adenomas (CA) and usual/atypical ductal hyperplasias (DH) of the breast for markers of TDIS (Supplementary Figure S4). Strikingly, we discovered that the great majority of epithelial cells in hyperplastic regions of CA and of DH displayed prominent 53BP1 foci (Figure 2A and B). This is in contrast to cells in normal epithelium adjacent to hyperplastic regions and cells in malignant cancers, which generally lacked 53BP1 foci (Figure 2A and B; Supplementary Figure S6A). Significantly, the great majority of DDR foci in cells of DH colocalized with telomeric repeats that were on average not shorter compared with other telomeres in these cells (Supplementary Figure S5A and B) and over 80% of cells in hyperplastic regions of the tissue were TIF positive (Figure 2C). As in premalignant melanocytic lesions, aberrant telomeric structures resembling fragile telomeres occasionally could be detected in TIF (Supplementary Figure S5B). TIF-positive cells could also be detected in CA, albeit at a lower frequency compared with DH (Supplementary Figure S5A). A likely reason is that telomeres in CA are very short, making it difficult to visualize telomeres using a PNA or antibodies against telomeric proteins (Meeker *et al*, 2004b) (Supplementary Figure S5C). Despite these limitations, we frequently detected dysfunctional telomeres and demonstrate a dramatic and statistically highly significant difference in TIF-positive cells between colonic adenomas and colonic carcinomas (42% versus 0.2%, respectively, $P<0.001$; Figure 2C). Although we did not detect aberrant telomeric structures in TIF of CA, likely due to the weak fluorescence signals emitted from telomeres, also in these premalignant lesions average lengths of telomeres in TIF were similar to the other telomeres in the cells (Supplementary Figure S5D). In contrast to cells in normal epithelium and in invasive carcinomas, 53BP1-positive cells in hyperplastic regions of CA and DH displayed elevated levels of macroH2A, providing further evidence that they were senescent (Figure 2D; Supplementary Figure S6A). As with melanocytic cells in nevi, epithelial cells that displayed high levels of macroH2A did not stain positive for the proliferation marker Ki67, corroborating our conclusions that macroH2A is a marker specific to senescent cells in tissues (Supplementary Figure S6B). Together, our data demonstrate hallmarks of TDIS in cells of precursor lesions to three distinct and common human cancers, but not in their malignant cancer counterparts.

Oncogenic H-RasV12 causes stalling of telomeric replication forks

Although telomere erosion in human cell cultures allows ~60 population doublings *in vitro*, the same number of cell divisions *in vivo* could potentially generate a lesion consisting of 1×10^{18} cells, a tumour mass weighing over 100 tons. We therefore reasoned that cells of precancerous lesions likely encountered stresses, which either accelerated telomere erosion or activated mechanisms that trigger telomere dysfunction. Common to all human cancer precursor lesions are stresses that lead to cellular hyperproliferation and DNA replication stress, often induced by aberrant oncogene signalling (Halazonetis *et al*, 2008). Since fragile sites are particularly sensitive to oncogene-induced DNA replication stress (Bartkova *et al*, 2006; Di Micco *et al*, 2006), and telomeres resemble fragile sites (Martinez *et al*, 2009; Sfeir *et al*, 2009; Ye *et al*, 2010), we asked whether oncogenic Ras causes DNA replication stress in telomeric repeats, thereby altering telomere structure and function. Using molecular DNA combing combined with telomeric fluorescence *in situ* hybridization (FISH; Figure 3A; Supplementary Figure S7A), we discovered that oncogene expression increased the fraction of DNA replication forks arresting at the transition between non-telomeric and telomeric tracts, compared with control cells (Figure 3B and C). In addition, oncogene-expressing cells accumulated partially replicated telomeres more frequently, while the numbers of fully replicated telomeres were reduced as compared with the control (Figure 3C). Indeed, the percentage of fork stalling events, defined as asymmetric DNA replication bubbles at telomeres (see Figure 3A), was dramatically increased by oncogene activation (Figure 3D). While these differences were statistically significant at telomeres ($P=0.03$), whole genome ana-

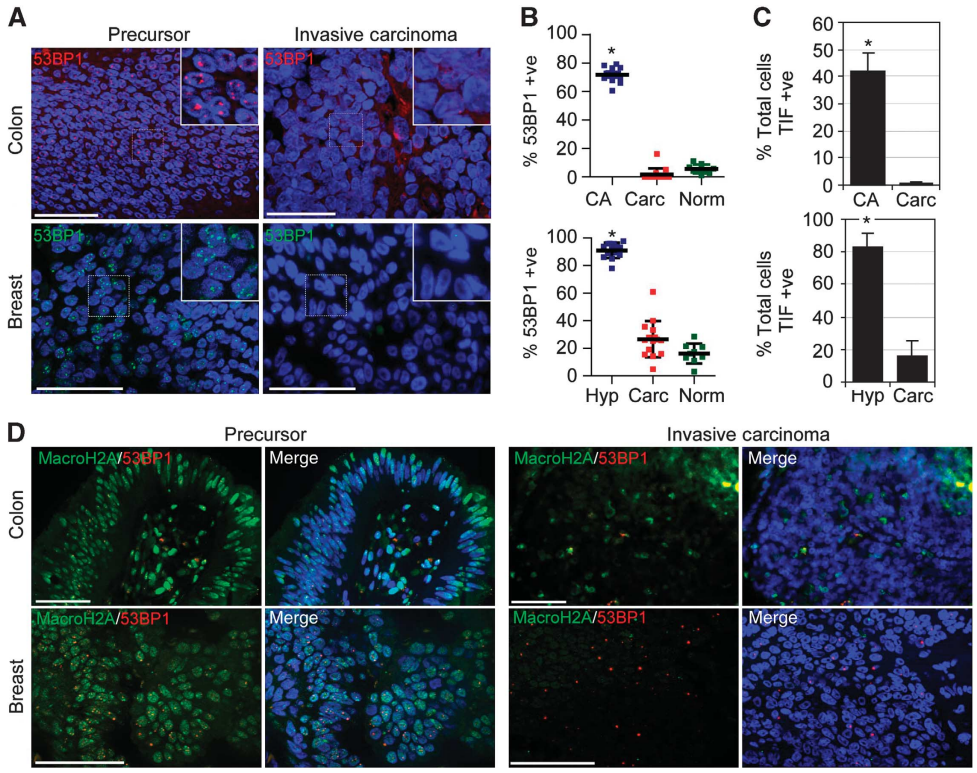

Figure 2 Epithelial cells of precursor lesions to colon- and breast-cancers display hallmarks of telomere dysfunction-induced cellular senescence. (**A**) Tissue sections from colonic adenomas (colon) and DH of the breast (breast; left column) and from invasive colon- and breast-carcinomas (right column) were immunostained with antibodies against 53BP1 (red, top row; green, bottom row). (**B**) Quantitation of 53BP1-positive epithelial cells (mean ± s.d). Top graph: colonic adenomas (CA, $n = 10$, 5588 cells), colonic adenocarcinomas (Carc, $n = 14$, 4898 cells), epithelial cells from adjacent normal colonic mucosa (Norm, $n = 9$, 2474 cells). Bottom graph: usual- and atypical-DH (Hyp, $n = 14$, 4359 cells), invasive ductal carcinomas (Carc, $n = 15$, 2905 cells), and luminal epithelial cells from adjacent normal ducts (Norm, $n = 9$, 3153 cells); $^*P < 0.001$ by one-way ANOVA followed by Tukey's *post hoc* test. (**C**) Quantitation of TIF-positive cells (mean ± s.d.). CA: $n = 10$; 3309 foci; Carc: $n = 14$; 205 foci; Hyp: $n = 14$, 1510 cells; Carc: $n = 15$, 661 cells; $^*P < 0.001$ by unpaired *t*-test. (**D**) Tissue sections from indicated lesions were immunostained using antibodies against 53PB1 (red) and macroH2A (green). Scale bar: 50 μm.

lysis revealed a more modest impact in response to oncogene activation (Supplementary Figure S7B), despite equal DNA labelling rates (Supplementary Figure S7C). Our data therefore demonstrate that telomeres are preferential sites of oncogene-induced DNA replication stress when compared with the rest of the genome.

Oncogenic H-RasV12 causes fragile telomeres and stochastic telomere attrition

DNA replication stress induced by drugs causes aberrant telomeric structures in metaphase, called fragile telomeres (Martinez *et al*, 2009; Sfeir *et al*, 2009). To determine whether Ras also causes telomeric replication stress, and hence fragile telomeres, we transduced contact inhibited cells with Ras and GFP using lentivirus, replated cells into colcemid containing medium and analysed telomeric structures in subsequent metaphases. In cells transduced with Ras during S-phase, but not in GFP-transduced cells, one quarter of all chromosome ends indeed displayed aberrant and fragile telomeres (Figure 4A). Fragile telomeres were observed similarly in hTERT-expressing BJ cells, demonstrating that hTERT does not suppress the fragile telomere phenotype caused by Ras overexpression (Suppementary Figure S8A). Surprisingly, in cells lacking hTERT activity, we also discovered that on many chromosomes the fluorescence signal intensities of sister telomeres were noticeably different, or undetectable, suggesting that Ras-induced DNA replication stress also causes stochastic telomere attrition (Figure 4A). In agreement with these observations, we demonstrate that cells expressing Ras for one S-phase consistently displayed ~40% fewer telomeric repeats compared with control cells as measured by FlowFISH (Figure 4B). Similar results were observed in cells that had undergone OIS (Supplementary Figure S8B). Ras did not preferentially shorten long or short telomeres as a reduction of telomere fluorescence signal was observed on all telomeres equally (Figure 4C). Ras-induced telomere shortening was not dependent on cellular growth arrest since expression of this oncogene in p53 knockdown cells, which are insensitive to OIS (Di Micco *et al*, 2006), also caused telomere attrition (Supplementary Figure S8C). However, while hTERT could not rescue stalling of telomeric replication forks in response to oncogenic signals, or the fragile telomere phenotype (see above), no telomere shortening could be detected in hTERT-expressing cells upon Ras expression (Supplementary Figure S8D). In summary, our data demonstrate that oncogenic signals cause DNA replication stress in telomeric repeats which leads to rapid, substantial, and stochastic telomere attrition in normal human somatic cells.

OIS is not stable in cells with high hTERT activity

In human cells, overexpression of oncogenic Ras causes cellular senescence following a brief period of hyperprolifera-

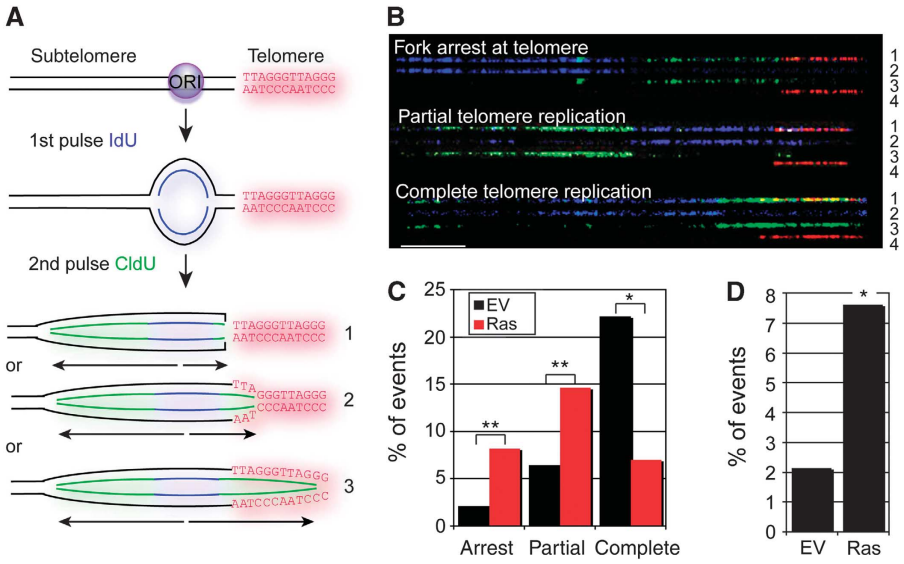

Figure 3 Oncogenic signals cause stalling of telomeric DNA replication forks. (**A**) Schematic illustrating a replication fork at the telomeric locus. Following pulse labelling of mouse fibroblasts with halogenated nucleotides, the DNA was extracted, combed, and processed by immunoFISH as indicated in Supplementary Figure S7. As an example, a newly fired DNA replication origin (ORI) that incorporates IdU during the first pulse (blue) is shown. CldU (green) is then incorporated during the second pulse. Telomeric repeats were detected using a Cy3-conjugated telomeric PNA (red). We interpret symmetric replication signals as normal replication fork progression (#3). Asymmetric DNA replication bubbles bordering, or extending into-telomeric repeats, as inferred by asymmetric replication signals were considered as telomeric fork stalling events (#1 and 2). These events were quantified in Figure 3D. (**B**) Representative images of analysed DNA replication patterns. Rows 1: merged image; 2: IdU (blue); 3: CldU (green); 4: telomere (red). Scale bar: 40 kb. (**C**) Quantitation of the percentage of DNA combing signals revealing DNA replication forks arrest at the start of a telomeric tract (within 2 kb), partial and complete telomere replication in empty vector- (EV; black bars; $n=140$) and H-RasV12-expressing (Ras; red bars; $n=171$) cells. $^{*}P<0.001$, $^{**}P=0.02$. (**D**) Quantitation of fork stalling events at telomeres in empty vector- (EV; $n=140$) and H-RasV12-expressing (Ras; $n=171$) cells. $^{*}P=0.03$.

tion regardless of hTERT expression status (Hahn *et al*, 1999a; Wei *et al*, 1999; Di Micco *et al*, 2006). The stability of Ras-induced senescence, however, is dependent on a variety of factors. For example, using freshly isolated human fibroblasts, or reducing the levels of reactive oxygen species (ROS), allows cells to bypass senescence despite high Ras expression levels (Lee *et al*, 1999; Benanti and Galloway, 2004; Sun *et al*, 2005). Similarly, reducing the levels of oncogenic H-Ras to those of endogenous wild-type Ras promotes cell growth, instead of arresting it (Tuveson *et al*, 2004; Sarkisian *et al*, 2007). In addition, overexpressing hTERT in cells that are insensitive to culture stresses also modulates the responses to oncogenes including H-RasV12 (Kohsaka *et al*, 2011; Sherman *et al*, 2011).

In agreement with these studies, we repeatedly observed that Ras did not induce a stable cellular growth arrest in multiple hTERT-expressing human fibroblasts strains and cells always continued to proliferate after arresting with a senescence-like phenotype for several days. To ensure that our hTERT-expressing cells had not acquired additional mutations preventing Ras from inducing a stable growth arrest, we cotransduced normal human fibroblasts with a combination of retroviruses expressing either, Ras and hTERT (Ras–hTERT), or Ras and empty vector (Ras–EV). Cells were selected for Ras expression only, reasoning that if hTERT facilitates escape from OIS, proliferating cells would emerge expressing both, Ras and hTERT. Consistent with previous observations (Hahn *et al*, 1999a; Wei *et al*, 1999; Di Micco *et al*, 2006) both retroviral combinations, Ras–EV and Ras–hTERT, caused cellular growth arrest early after retroviral transduction as demonstrated by growth curves and BrdU incorporation assays (Figure 5A and B). While empty vector transduced cells displayed a modest increase in DDR foci early after transduction, likely due to stresses caused by the retroviral transduction process, Ras-expressing cells showed a dramatic increase in cells that displayed multiple DDR foci, which is consistent with previous studies (Di Micco *et al*, 2006) (Figure 5D; Supplementary Figure S9A). Only 25% of all DDR foci in both, Ras–EV and Ras–hTERT cells colocalized with telomeric sequences, demonstrating that Ras-induced DNA replication stress causes DDR foci primarily at non-telomeric sequences, and to a lesser extent also in telomeric repeats (Figure 5E; Supplementary Figure S9B). However, as we continued to characterize cultures for an additional 3 weeks after Ras-expressing cells entered senescence, we observed that the percentage of cells with multiple DDR foci decreased slightly in Ras–EV cells but decreased substantially in Ras–hTERT cultures (Figure 5D). Significantly, as the average number of 53BP1 foci per cell nucleus decreased over this time in senescent Ras–EV cells, the colocalizations between 53BP1 foci and telomeres increased, reaching levels of over 50% (Figure 5E; Supplementary Figure S9C). Our data therefore demonstrate that Ras causes DDR foci at both non-telomeric and telomeric DNA sequences. However, while non-telomeric DDR foci decreased over time in senescent cells that lack telomerase activity, DDR foci at telomeric repeats persisted. Since telomeres with persistent DDR foci are defined as dysfunctional, our data therefore demonstrate that oncogenic Ras causes telomere dysfunction in normal human cells. Similar to dysfunctional telomeres in cancer precursor lesions, the telomeres that colocalized with these persistent 53BP1 foci were not shorter compared with

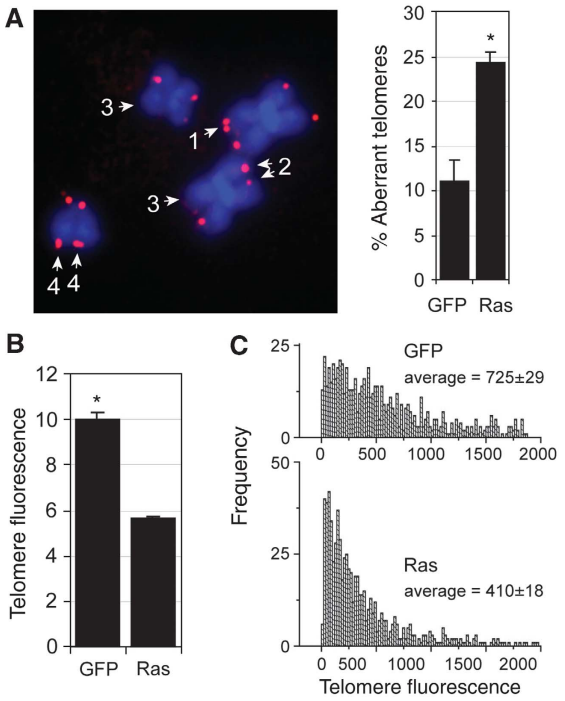

Figure 4 Oncogenic signals cause fragile telomeres and stochastic telomere attrition. (**A**) Metaphases from BJ cells that were contact inhibited, transduced with lentivirus encoding Ras, and subsequently released into colcemid containing medium. Chromosome ends, labelled using a telomeric Cy3-conjugated-PNA (red), either displayed telomeric doublets (1), different signal intensities on sister chromatids (2), absence of signal (3), or diffuse telomeric staining patterns (4). Bar graph: percentage of aberrant telomeric structures (± s.d.) in GFP (69 metaphases) and Ras (98 metaphases) expressing cells ($n = 3$); $^*P < 0.001$. (**B**) Contact inhibited BJ cells were transduced with lentivirus encoding GFP (control) or Ras followed by release into colcemid-containing medium. Telomere fluorescence (arbitrary units, mean ± s.d.) as measured by flow-FISH or q-FISH (**C**) in Ras- and GFP-transduced cells; $^*P < 0.001$. Statistical significance was calculated by unpaired *t*-test.

the other telomeres in the same cells, suggesting that Ras-induced telomere dysfunction was not exclusively due to critical telomere attrition (Supplementary Figure S9D). In contrast to normal cells whose growth was severely compromised due to Ras expression, Ras–hTERT-expressing cells continued to proliferate 1 week after they entered a senescence-like state, and cells displayed higher proliferation rates compared with hTERT control cultures, low levels of DDR foci, high telomerase activity, and elevated levels of Ras (Figure 5A–D; Supplementary Figure S9E). The ability of hTERT to destabilize Ras-induced senescence required its catalytic activity, since cells expressing a catalytically inactive dominant negative form of hTERT (DN-hTERT; Supplementary Figure S9H) (Hahn *et al*, 1999b) stably arrested following Ras expression as a result of telomere dysfunction (Supplementary Figure S9F and G).

To test whether oncogenes other than H-RasV12 also affect telomere structure and function, we retrovirally transduced normal human cells and hTERT-expressing cells with B-Raf harbouring the V600E amino-acid substitution (Hao *et al*, 2007), an oncogenic mutation that is observed in the great majority of human nevi and in some precursors lesions to colorectal carcinomas, among others (Michaloglou *et al*, 2008). Consistent with previous observations (Michaloglou *et al*, 2005), we show that BRafV600E expression caused growth arrest of both normal human cells and hTERT-expressing cells after a brief period of proliferation (Supplementary Figure S10A and B). Growth arrested BRafV600E-expressing cells displayed a high degree of γH2AX foci demonstrating activation of a DDR (Supplementary Figure S10D). The proliferative arrest was preceded by the appearance of fragile and aberrant telomeric structures detected on metaphase chromosomes, demonstrating that also this oncogene causes telomeric replication stress (Supplementary Figure S10C). Similar to Ras-expressing cells, the proliferative arrest triggered by BRafV600E was not stable in hTERT-expressing cells and BRafV600E/hTERT-expressing cells eventually continued to proliferate with high BRafV600E expression levels. This was in contrast to cells lacking hTERT expression, which arrested stably due to a persistent telomeric DDR (Supplementary Figure S10). Overall, our data therefore demonstrate that telomere dysfunction stabilizes an otherwise transient growth arrest induced by oncogenic signals.

DNA replication stress causes TDIS in normal somatic cells that lack hTERT activity

To directly test whether DNA replication stress causes TDIS in normal human cells, we incubated BJ fibroblasts with low doses of hydroxyurea (HU) and aphidicolin (Aph) for 4 days. Under these conditions cells entered, or proceeded through S-phase, as detected by BrdU incorporation (Supplementary Figure S11A). While normal cells accumulated one or more DDR foci in response to drug treatment, hTERT-expressing cells did not, suggesting that observed DNA damage was a result of telomere dysfunction (Figure 6A; Supplementary Figure S11B and C). Indeed, almost all of the DDR foci remaining after 4 days of drug treatment colocalized with telomeric DNA repeats and therefore caused cells to become TIF positive, demonstrating that drug-induced DNA replication stress caused telomere dysfunction in cells that lack hTERT (Figure 6B; Supplementary Figure S11D). After drug removal, most cells lacking hTERT did not incorporate BrdU, demonstrating that DNA replication stress caused TDIS in normal cells (Figure 6C; Supplementary Figure S11E). Significantly, since the presence of telomerase reduced formation of telomeric DDR foci in response to DNA replication stress (Figure 6B), but does not prevent DNA replication fork stalling in telomeric repeats (Figure 3; Supplementary Figure S8A), our data also suggest that one function of hTERT is to prevent telomere dysfunction in response to stalled DNA replication forks. Finally, to further corroborate our conclusions that dysfunctional telomeres in human cancer precursor lesions were caused by telomeric replication stress, we immunostained human cancer precursor lesions with antibodies against ATR phosphorylated at serine 428, a posttranslational modification that is associated with DNA replication stress-induced DDR foci (Robinson *et al*, 2009) (Supplementary Figure S12). We show that DDR foci, which are primarily telomeric (Figures 1 and 2), included P-ATR(S428) (Figure 6D) supporting our conclusions that TDIS in human cancer precursor lesions was a consequence of oncogene-induced DNA replication stress.

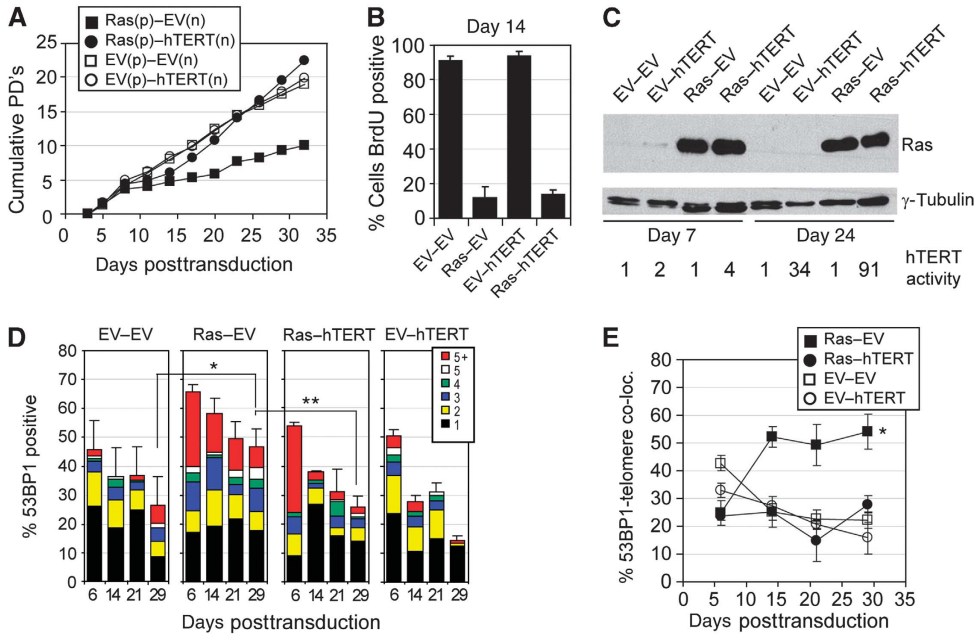

Figure 5 Oncogenic Ras causes transient non-telomeric- and persistent-telomeric DDR foci in non-telomerized human cells. (**A**) Growth curve of BJ cells transduced with indicated retroviral combinations. Experiments were performed a total of five times (three times in BJ cells and two times in unrelated normal human foreskin fibroblasts) with similar results. p: encoding puromycin resistance; n: encoding neomycin resistance. Note that cells were selected using puromycin only. (**B**) Percentage of BrdU-positive cells 14 days following transduction (or 12 days following removal of the selection drug puromycin; BrdU added for 48 h). (**C**) Immunoblot showing Ras expression levels in BJ cells at indicated days following retroviral transduction. γ-Tubulin served as a loading control. Numbers represent relative telomerase activity following retroviral transduction, as measured by TRAPeze assay. (**D**) BJ cells were transduced with indicated combinations of retroviruses and analysed for the percentages of 53BP1-positive cells (± s.d.) at indicated times after transduction. Colour bars indicate the frequency of 53BP1 foci per cell nucleus. At least 100 cells were analysed for each group and time point; $*P = 0.001$; $**P = 0.004$ by unpaired *t*-test. (**E**) Percentage of 53BP1 (± s.d.) foci colocalizing with telomeric DNA at indicated times after transduction of indicated retroviral combinations. Only DDR-positive cells were analysed. A minimum of 30 cells were analysed for each group and time point (average of 165 53BP1 foci/group and time point); $*P < 0.001$ by repeated measures one-way ANOVA.

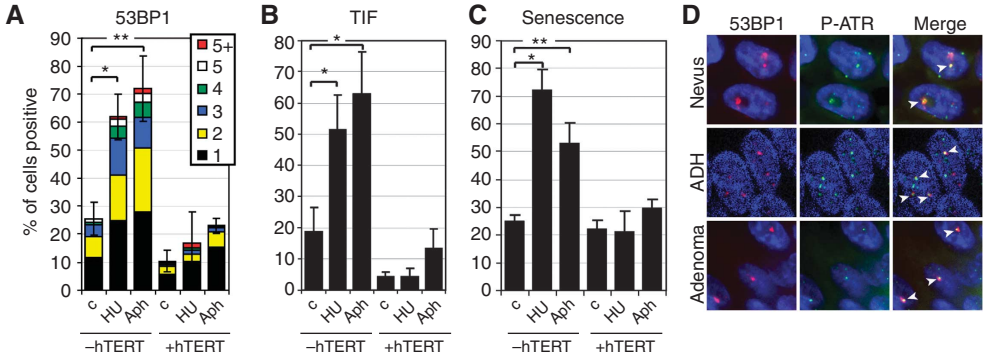

Figure 6 DNA replication stress causes TDIS in normal human cells. (**A**) BJ cells and hTERT-expressing BJ cells were incubated with low concentrations of hydroxyurea (HU; 50 μM) and aphidicolin (Aph: 0.3 μM) for 4 days followed by a release from the block for 48 h. Bar graph: percentage of 53BP1-positive cells (± s.d.). The frequency of DNA damage foci per cell nucleus is indicated with coloured bars. A minimum of 400 cells per group were analysed ($n = 3$); $*P = 0.002$, $**P < 0.001$. (**B**) Percentage of TIF-positive cells (± s.d.). A minimum of 100 cells per group were analysed ($n = 3$); $*P < 0.001$. (**C**) Percentage of cells that did not incorporate BrdU over a 48 h labelling period and were therefore considered senescent (± s.d.). BrdU was added to the culture medium following drug removal. A minimum of 400 cells per group were analysed ($n = 3$); $*P = 0.007$, $**P = 0.012$. (**D**) Colocalization between 53BP1 (red) and ATR(Ser428; P-ATR) foci in nevi (top row), ADH (middle row), and colonic adenomas (bottom row). White arrows indicate colocalizations. Statistical significance was calculated by paired *t*-test.

Discussion

While TDIS has been demonstrated to limit tumour growth in animal model systems (Cosme-Blanco *et al*, 2007; Feldser and Greider, 2007), the relevance of these observations for human disease has remained elusive. Our observation that three common, yet distinct, human cancer precursor lesions are comprised of cells that display hallmarks of DNA replication stress-induced TDIS suggests that TDIS is an *in vivo* physiological mechanism that prevents progression of cancer in humans. Significantly, short telomeres and signs of a DDR are also observed in other cancer precursor lesions (Meeker *et al*, 2004b; Bartkova *et al*, 2005; Gorgoulis *et al*, 2005), indicating that TDIS could limit growth of many

human cancers. In line with previous studies demonstrating the role of telomeres in evolving human and mouse model systems (Chin *et al*, 1999, 2004; Rudolph *et al*, 2001), we thus propose that TDIS, along with other telomere checkpoints such as apoptosis (Chin *et al*, 1999; Qi *et al*, 2003; Wong *et al*, 2003), serves as a critical tumour suppressing mechanism in humans by restraining cancer progression at premalignant stages (Figure 7).

Our data demonstrating that dysfunctional telomeres in human cancer precursor lesions on average were not detectably shorter compared with other telomeres in these lesions were unexpected. While we cannot rule out the possibility that the few DDR foci lacking colocalizations with telomeric signals are at chromosome ends that completely lack telomeric repeats, our data suggest that most dysfunctional telomeres in these lesions still retain significant numbers of repeats. Based on recent studies demonstrating that telomeric DSBs are irreparable and consequently result in dysfunction of telomeres that are not necessarily short (Fumagalli *et al*, 2012), our data suggest that the reasons for telomere dysfunction in cells of human cancer precursor lesions was not due to critical telomere erosion, but rather due to formation of telomeric DNA lesions as a result of oncogene-induced DNA replication stress. This is supported by our results demonstrating features of DNA replication stress at dysfunctional telomeres in cancer precursor lesions, such as telomeric doublets and P-ATR foci.

While most telomeres in cells of nevi are long, as judged by the fluorescence signal intensities emitted from the telomeric probe (Figure 1D; Supplementary Figure S2A), total telomere lengths in cells of epithelial cancer precursors appeared significantly shorter compared with surrounding stromal cells (Supplementary Figure S5C), consistent with previous observations (Meeker *et al*, 2004a, b; Michaloglou *et al*, 2005). Despite these differences in total telomere lengths, all cells displayed hallmarks of TDIS. Our data therefore suggest that cells in epithelial lesions had undergone more cumulative population doublings, and consequently

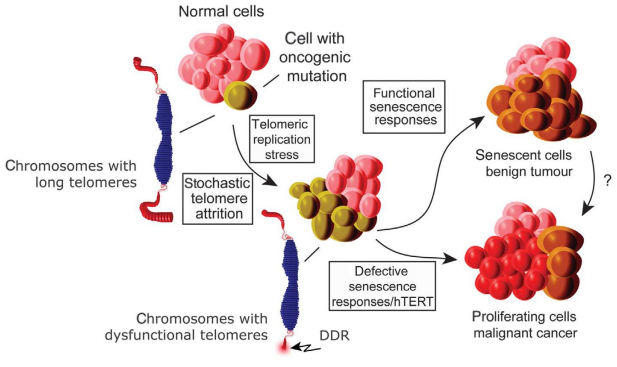

Figure 7 Model illustrating the role of TDIS in suppressing malignant cancer progression in humans. Cells encountering oncogenic signals are exposed to telomeric replication stress, which leads to stochastic telomere attrition and telomere dysfunction in cells that lack telomerase activity. In normal somatic cells, telomere dysfunction results in cellular senescence, thereby preventing malignant cancer progression. In contrast, telomere dysfunction is suppressed in cells with high telomerase activity allowing these cells to continue proliferating. Similarly, in cells with compromised senescence responses, telomere dysfunction generates chromosomal instability, an event that is associated with reactivation of telomerase and malignant cancer progression.

contained shorter telomeres, compared with cells melanocytic cells in nevi. Significantly, most senescent cells in nevi displayed only 1–2 DDR foci, while senescent cells in ductal hyperplasias and colonic adenomas displayed many more DDR foci per cell nucleus (e.g., compare Figures 1A and 2A). Thus, it is likely that melanocytic cells are more sensitive to a telomeric DDR compared with cells in epithelial tissues and consequently arrest earlier in response to telomere dysfunction. Supporting this conclusion are studies demonstrating that cultured mammary epithelial cells continue to proliferate despite displaying few dysfunctional telomeres, and only undergo replicative senescence once many more telomeres in the cell had become dysfunctional (Beliveau *et al*, 2007). In contrast, other cell types such as fibroblasts undergo senescence due to only one, or very few dysfunctional telomeres (Herbig *et al*, 2004; Abdallah *et al*, 2009). While the reasons for these differences are currently unknown, it is tempting to speculate that the decreased sensitivity to dysfunctional telomeres is a feature of cells in highly proliferative tissues such as colon and breast. This would allow these cells to tolerate occasional DNA replication defects in telomeric repeats without arresting prematurely and impeding tissue growth.

Our data demonstrating high DDR activity in cancer precursor lesions and low activity in malignant cancers is consistent with previous observations (Bartkova *et al*, 2005, 2007; Gorgoulis *et al*, 2005; Nuciforo *et al*, 2007). The suppression of the DDR in malignant cancers has previously been attributed to the inactivation or loss of expression of certain DDR factors at later stages during cancer progression. In addition, a recent study demonstrated that DDR signalling in proliferating oncogene-expressing cells is also restrained by the formation of senescence-associated heterochromatic foci (SAHF) (Di Micco *et al*, 2011). Our data now suggest that hTERT also contributes to this low DDR activity observed in malignant cancers by suppressing the formation of telomeric DDR foci caused by oncogene-induced telomeric replication stress. Consistent with this interpretation are observations that cells in early cancer precursor lesions generally display low or absent telomerase activity, whereas cells in over 90% of all human malignant cancers have reactivated this enzyme to maintain telomere lengths and function (Artandi and DePinho, 2010). hTERT counteracts a telomeric DDR, both by preventing critical telomere shortening and by suppressing the formation of replication stress-induced telomeric DDR foci (Figures 5 and 6, Supplementary Figure S10). Thus, the dramatically reduced number of cells with DDR foci in analysed malignant lesions likely is also a consequence of increased hTERT activity in these cancers. Supporting this conclusion are data demonstrating that telomerase inhibition can lead to an increased formation of DDR foci and an ATM-dependent growth arrest in hTERT-positive human cancer cells (Djojosubroto *et al*, 2005; Wong *et al*, 2009). Therefore, inhibitors of telomerase will likely prove to be a valuable tool to combat cancers that retain the ability to undergo TDIS or telomere dysfunction-induced apoptosis.

In optimal environments, somatic human cells gradually lose telomeric sequences until TDIS limits further cell proliferation. Gradual telomere erosion is a consequence of the 'end replication problem', postreplicative nucleolytic processing of chromosome ends, and events that delete telomeric

repeats in a sporadic manner. Stresses that likely contribute to telomere erosion include increased levels of ROS, DNA replication errors in telomeric repeats, and defects in proteins involved in telomere maintenance (Lansdorp, 2005). We now demonstrate that oncogenic signals also cause stochastic telomere attrition and dysfunction in cells lacking hTERT activity. Since oncogenes cause DNA replication stress, which frequently leads to the collapse of DNA replication forks and consequently DSBs at fragile sites (Bartkova *et al*, 2005, 2006; Arlt *et al*, 2006; Di Micco *et al*, 2006), and telomeres resemble fragile sites (Martinez *et al*, 2009; Sfeir *et al*, 2009; Ye *et al*, 2010), it is likely that oncogene-induced telomere attrition and dysfunction is due to DNA replication stress in telomeric repeats. Indeed, we show that DNA replication forks prematurely terminated in telomeric repeats preferentially in Ras-expressing cells (Figure 3), causing dramatic and stochastic telomere attrition even within one cell division cycle (Figure 4). Oncogene expression also caused a high degree of both non-telomeric and telomeric DDR foci, likely due to DNA repair events at collapsed replication forks. Consistent with the recent discovery that telomeric DSB's resist DNA repair (Fumagalli *et al*, 2012), our data demonstrate that telomeric DDR foci persisted in cells lacking hTERT activity while non-telomeric foci were resolved within days (Figure 5D; Supplementary Figure S10). Since hTERT-expressing cells were able to resolve DDR foci, allowing them to eventually continue growth, we conclude that the primary reason for cellular senescence in oncogene-expressing cells that lack high telomerase activity is due to persistent telomeric DDR foci. OIS is therefore a cellular stress response that is stabilized by dysfunctional telomeres. Furthermore, based on our data we suggest that, rather than acting as cell division-count down timers, telomeres function as sentinels of genotoxic and hyperproliferative stresses that stabilize cellular senescence once their structure is compromised. In humans, TDIS is both critical and highly effective as this tumour suppressing mechanism appears to limit malignant cancer progression in multiple and distinct tissues.

Materials and methods

Human cancer tissue samples

Archival and paraffin-embedded tumour tissue was obtained from the tumour tissue bank at NJMS-University Hospital with the approval of the local IRB committee. Haematoxylin and eosin-stained tissue sections were analysed and labelled by an experienced pathologist. Imaging, counting, and statistical analysis was performed independently by two individuals. No patients were treated with radiation or chemotherapy prior to surgical resection of tumour tissue.

Cell culture

BJ cells were cultured in Ham's F10 nutrient mixture (Life Technologies) supplemented with 15% batch-tested fetal bovine serum (Atlanta Biologicals, Lawrenceville, GA), 20 mM L-glutamine (Cellgro, Manassas, VA), and penicillin/streptomycin (100 U/ml penicillin and 100 μg/ml streptomycin; Cellgro, Manassas, VA). Cultures were passaged using a 1:4 subculture regimen and incubated at 37°C in an atmosphere of 5% CO_2. Cells were labelled with 1 μg/ml BrdU. Aphidicolin (Sigma, St Louis, MO; 0.3 μM) and hydroxyurea (Sigma, St Louis, MO; 50 μM) were directly added to the culture medium. Growth curves were generated using a hemocytometer and the formula $PD = \log2(N_{final}/N_{initial})$ where $N_{initial}$ is the number of cells seeded at each passage and N_{final} is the number of cells recovered from the dish. NIH3T3 mouse embryonic fibroblasts (MEFs) were cultured under standard conditions. pBABE-Puro H-RasV12 and corresponding empty vector pBABE-Puro were used to infect cells by retroviral transduction as in (Di Micco *et al*, 2006). Four days after infection, cells were labelled with thymidine analogues for DNA combing studies.

Microscopy

Images were acquired using a Zeiss Axiovert 200M microscope, an AxioCamMRm camera (Zeiss), and AxioVision 4.6.3 software (Zeiss). To analyse and quantitate colocalization between telomere signals and 53BP1 foci, images were acquired as *z*-series through the entire thickness of the specimen (10–15 images, 0.3–0.4 μm optical slices) using a motorized stage, a ×100/1.4 oil immersion lens, and an ApoTome (Zeiss). ApoTome microscopy eliminates out of focus light and generates shallow focal planes (0.4 μm using a ×100 oil objective). To quantitate 53BP1 foci, images were acquired through the entire specimen as *z*-stacks using a ×63/1.4 oil immersion lens and an ApoTome. Stacks were merged into a single image using the AxioVision software for easier counting.

Immunofluorescence and ImmunoFISH

Cultured cells were processed for immunofluorescence analysis as described previously (Herbig *et al*, 2004). Deparaffinized 4-μm tissue sections were incubated in sodium citrate buffer (10 mM Na–citrate, 0.05% Tween 20, pH = 6) at 95°C for 45 min to retrieve antigens. Tissue sections were subsequently rinsed with water and incubated with block buffer (4% BSA in PBS + 0.1% Tween 20) for 30 min. Primary antibodies were incubated overnight at 4°C in block buffer at indicated concentrations (see below). Following 2 × 5 min washes with PBST, tissue sections were incubated with secondary antibodies as indicated (1:1000 in block buffer) for 1 h at room temperature. Slides were washed 3 × 5 min with PBST, rinsed with water and mounted using DAPI containing mounting medium (Vector Laboratories, Burlingame, CA).

To detect TIF, tissue sections were deparaffinized and heat treated in sodium citrate buffer as described above. Sections were dehydrated by placing them in 95% ethanol for 3 min. After air-drying, nuclear DNA was denatured for 5 min at 80°C in hybridization buffer containing Cy3-conjugated telomere-specific PNA (Cy3-$(C_3TA_2)_3$; Panagene, Korea) at 0.5 μg/ml, 70% formamide, 12 mM Tris–HCl pH = 8.0, 5 mM KCl, 1 mM $MgCl_2$, 0.08% Triton X-100 and 0.25% acetylated BSA (Sigma-Aldrich, St Louis, MO), followed by incubation in the same buffer for 2 h at room temperature. Slides were washed sequentially with 70% formamide/0.6 × SSC (90 mM NaCl, 9 mM Na–citrate (pH = 7); 3 × 15 min), 2 × SSC (1 × 15 min), PBS (5 min), PBST (PBS + 0.1% Tween 20; 5 min), and incubated with block buffer (4% BSA in PBST) for 30 min. Immunostaining using primary polyclonal anti-53BP1 antibodies and secondary Alexa Fluor 488-conjugated goat anti rabbit antibodies (Invitrogen, Carlsbad, CA) was performed as described above.

Telomere length measurements by quantitative FISH and FISH with flow cytometry (flow-FISH)

Cultured cells were arrested at mitosis by treatment with colcemid (0.1 μg/ml). Cells were subsequently incubated with a hypotonic solution of potassium chloride at 37°C for 15 min followed by fixation in Carnoy's fixative. Quantitative FISH (qFISH) was performed using telomere sequence-specific PNA probe labelled with Cy3 as described (Hande *et al*, 1999). Metaphase spreads for different samples were hybridized simultaneously. To avoid selection bias, good and well spread metaphases were randomly chosen for analysis. Images were acquired on the same day (within 3 h) for all the samples using the Zeiss Axioplan 2 imaging fluorescence microscope. Fluorescence intensity of telomere signals was measured using the *in situ* imaging software (Metasystems, Germany). The total amount of telomere DNA was also measured at the single-cell level by flow-FISH as described (d'Adda di Fagagna *et al*, 1999; Poonepalli *et al*, 2005). Briefly, control and experimental cells were suspended in the hybridization buffer containing fluorescein isothiocyanate (FITC)-labelled telomere-specific PNA probe. After denaturation at 86°C for 10 min, hybridization was carried out at room temperature for 2 h. Unbound telomere PNA probe was removed by posthybridization washes and the cells were counterstained with propidium iodide. Telomere fluorescence was subsequently measured on a flow cytometer using argon ion laser (488 nm) to excite FITC. FITC-labelled fluorescent calibration beads (QuantumTM-24 Premixed; Flow Cytometry Standards Corporation, San Juan, Puerto Rico)

were used to correct for daily shifts in the linearity of the flow cytometer and fluctuations in the laser intensity and alignment and to express the results in standard fluorescence units. The resulting calibration curve was then used to convert telomere fluorescence data to molecules of equivalent soluble fluorochrome units (MESF), allowing comparison of results between experiments. Hela cells were used as biological control in each set of experiment to correct any experimental variations. Both qFISH and flow-FISH studies were carried out blind. In tumour tissue, relative telomere lengths were assessed by quantification of telomeric signal fluorescence intensities using the ImageJ software (version 1.45) and the object counter 3D plugin on consecutive *z*-stacks acquired using a Zeiss Axiovision 200M microscope equipped with ApoTome.

Analysis of DNA replication dynamics at telomeres by DNA combing and FISH

MEFs were sequentially labelled with 25 μM IdU for 1 h followed by 25 μM CldU for an additional hour in the culture medium. Cells were then washed three times in PBS and incubated 3 h in media without IdU/CldU. This procedure was repeated three times. DNA combing was performed as previously described in Lebofsky and Bensimon (2003). Cells were then embedded in agarose plugs, proteinase K-treated and DNA extracted. DNA was combed on silanised coverslips. Telomeres were detected with a Cy3-conjugated Telomere PNA probe (Cy3-OO-(CCCTAA)3; Panagene, Korea) by FISH as described in Hande *et al* (1999), with the only modification of a DNA denaturation step in 0.5 M NaOH 1 M NaCl for 8 min. Halogenated nucleotides were detected with specific primary antibodies (IdU: mouse anti-BrdU, Becton Dickinson; CldU: rat anti-BrdU, Abcam) and secondary antibodies (Alexa Fluor 647-conjugated goat anti-mouse, Molecular Probes; Alexa Fluor 488-conjugated goat anti-rat, Molecular Probes). Images were acquired with a fluorescence microscope and labelled DNA molecules were individually manually measured in a blind manner by ImageJ software and analysed by Excel.

Immunoblotting

Protein extracts were prepared in lysis buffer (20 mM Hepes-KOH, pH 7.9, 0.42 M KCl, 25% glycerol, 0.1 mM EDTA, 5 mM $MgCl_2$, 0.2% NP40, 1 mM DTT, and 500 μM PMSF and 1:100 protease inhibitor cocktail). In all, 10 μg protein samples were run on 10% SDS–PAGE gels and proteins were transferred to PVDF membranes (Pall Life Sciences, Pensacola, FL) using a Bio-Rad mini Trans-Blot Cell at 350 mA for 90 min. After transfer, membranes were blocked in 5% non-fat dry milk in 1 × TBST (150 mM NaCl, 10 mM Tris–HCl, pH 8.0, 0.05% Tween 20) at room temperature for 1 h, then incubated with primary antibody at 4°C overnight with shaking. Membranes were washed three times in 1 × TBST for 10 min with shaking, then incubated with HRP-conjugated goat anti-mouse or goat anti-rabbit secondary antibodies (Pierce Biotechnology, Rockford, IL) at room temperature for 1 h with shaking. Membranes were washed three times in 1 × TBST for 10 min. Proteins were detected with a SuperSignal West Pico Chemiluminescent Substrate (Pierce Biotechnology, Rockford, IL) and signals were exposed to Hyblot CL Autoradiography films (Denville, Mutuchen, NJ).

Telomerase activity

Telomerase activity was measured by the TRAPEZE® RT Telomerase detection Kit (Millipore, Bedford, MA), utilizing PCR and Amplifluor primers according to the manufacturer's instructions. Briefly, pelleted cells were resuspended in lysis buffer, incubated on ice for 30 min and spun to collect the supernatant. The fluorometric detection of telomerase activity of the supernatant equivalent to 1000 cells was detected using 7300 Real Time PCR system (Applied Biosystems, Foster City, CA). Quantitative values of the telomerase activity were obtained from a standard curve generated by using dilutions of control template provided by the kit.

Viral transductions

Retrovirus was generated using the pBabe-puro and pBabe-hygro vectors (Morgenstern and Land, 1990) and the Phoenix amphotropic virus packaging cell line. The sources of the plasmids were as follows: pBabe H-RasV12 puro, Addgene plasmid 1768; pBabe BRafV600E-puro and pBabe-puro: Addgene plasmids 17544 and 1764, respectively. High titre retrovirus was incubated with 30–40% confluent BJ cells for 48 h. Cells were selected with 2 μg/ml puromycin (Sigma-Aldrich, St Louis, MO) for 48–72 h. Lentivirus was generated in 293T cells by calcium phosphate transfection of pRRL.SIM-18 containing either GFP or H-RasV12 together with pMDL g/pRRE, pVSVG, pRSV-REV (kind gift from J Campisi). BJ cells were contact inhibited for 7 days and transduced with GFP or H-RasV12-expressing lentivirus. After 72 h, cells were replated into colcemid containing medium (0.1 μg/ml; Invitrogen, Carlsbad, CA), and telomere length was analysed by q-FISH 48 h following release from contact inhibition.

Antibodies

The sources and dilutions of antibodies used were as follows: macroH2A1.2 (1:2000) and monoclonal 53BP1 antibodies have been reported (Schultz *et al*, 2000; Zhang *et al*, 2007); BrdU (GE Health, Piscataway, NJ; 1:200), 53BP1 (monoclonal; Chemicon, Temecula, CA; 1:250), 53BP1 (polyclonal; Novus, Littleton, CO; 1:500), TRF2 (IMGENEX, San Diego, CA; #IMG-124A), Melan-A (Santa Cruz, Santa Cruz, CA; 1:200), p16 (H-154; Santa Cruz, Santa Cruz, CA; 1:200); γH2AX(S139) (Upstate, Chicago, IL; 1:1000); anti-centromeric proteins (Antibodies, Davis, CA; 1:500); Ki67 (polyclonal, Abcam, Cambridge, MA; 1:100 and monoclonal, BD Biosciences, San Jose, CA, 1:100); P-ATR(Ser428) (Cell Signaling, Danver, MA; 1:100); p53 (DO-7; Novocastra); Ras (BD Transduction Laboratories, San Jose, CA; 1:1000); hTERT (polyclonal; Rockland, Gilbertsville, PA; 1:500), Raf-B (F-7) sc-5284 (monoclonal; Santa Santa Cruz Biotech, Santa Cruz, CA; 1:500); γ-Tubulin (Sigma, St Louis, MO; 1:5000).

Statistical analysis

The observed data are normally distributed (Shapiro–Wilk *W* test) and presented as mean values ± s.d. To approximate normal distribution, the percentage of 53BP1-positive cells in melanoma group were log-transformed for data analyses and back transformed for data presentation. The differences between groups were tested using the unpaired (independent samples) or paired samples (for paired data) Student's *t*-test or one-way analysis of variance (ANOVA) analysis followed by Tukey's *post hoc* test for multiple comparisons as indicated. ANOVA with repeated measurements followed by *post hoc* analysis with Bonferroni's correction for multiple comparisons allowed us to test changes in percentage 53BP1-telomere colocalization during days posttransduction and difference between groups. Simple correlation analyses were applied to evaluate the relationship between patient age and the percentages of 53BP1-positive cells in different groups as indicated. All *P*-values presented are two-tailed and a $P<0.05$ was chosen for levels of significance. Statistical analyses were performed using SPSS 16 software package (SPSS, Inc., Chicago, IL) or GraphPad Prism software version 5.0 (San Diego, CA, USA).

Supplementary data

Supplementary data are available at *The EMBO Journal* Online (http://www.embojournal.org).

Acknowledgements

We are grateful to P Adams for generously providing the anti-macroH2A1.2 antibodies, A Bensimon and J Komatsu for help with DNA combing, and D Parazzoli for DNA fibres images acquisition. The monoclonal anti-53BP1 antibody was a kind gift from TD Halazonetis. Retroviral vectors pBabe-hTERT-neo was generously provided by J Santos. pBabe-hTERT-puro (wt and DN) and pBabe-H-RasV12 were provided by R Weinberg. pBabe B-RafV600E was from C Der. UH was supported by the New Jersey Commission on Cancer Research (09-1124-CCR-EO), a New Scholar in Aging Award from The Ellison Medical Foundation (AG-NS-0387-7), and by the NCI (R01CA136533). MPH acknowledges the grant support from Academic Research Fund, Ministry of Education, Singpaore (T206B3108). Work in FdAdF laboratory was supported by AIRC (Associazione Italiana per la Ricerca sul Cancro), European Community's 7th Framework Programme (FP7/2007–2013) under grant agreement no. 202230, acronym

'GENINCA', HFSP (Human Frontier Science Program), AICR (Association for International Cancer Research), EMBO Young Investigator Program and Telethon. AC was supported by Fondazione Umberto Veronesi (FUV).

Author contributions: AS generated data in Figures 1, 2, and 6D, Supplementary Figures S1B–F, S2, S3, S5, and S6A and B; JK generated data in Figures 5D–E and 6A–C, Supplementary Figures S9A–D, S11, and S12; PLP generated data in Supplementary Figures S9E–H and S10; HR generated data in Figures 4A and B and 5A–C, Supplementary Figure S8D; NM generated data in Supplementary Figures S1A and S4; AC performed experiments for Figure 3 and Supplementary Figure S7; MF performed experiments for Figure 4C; RDM performed experiments for Supplementary Figure S8B and C; VB performed statistical analysis; RLG and MPH generated data for Figure 4B and C, Supplementary Figure S8B–D; FdAdF designed Figures 3 and 4C, Supplementary Figures S7 and S8B and C experiments and discussed the results. UH generated data in Supplementary Figure S8A, planned the project, wrote the manuscript, and assembled all images.

Conflict of interest

The authors declare that they have no conflict of interest.

References

Abdallah P, Luciano P, Runge KW, Lisby M, Geli V, Gilson E, Teixeira MT (2009) A two-step model for senescence triggered by a single critically short telomere. *Nat Cell Biol* **11:** 988–993

Adams MM, Carpenter PB (2006) Tying the loose ends together in DNA double strand break repair with 53BP1. *Cell Div* **1:** 19

Arlt MF, Durkin SG, Ragland RL, Glover TW (2006) Common fragile sites as targets for chromosome rearrangements. *DNA Repair (Amst)* **5:** 1126–1135

Artandi SE, DePinho RA (2010) Telomeres and telomerase in cancer. *Carcinogenesis* **31:** 9–18

Augereau A, T'Kint de Roodenbeke C, Simonet T, Bauwens S, Horard B, Callanan M, Leroux D, Jallades L, Salles G, Gilson E, Poncet D (2011) Telomeric damage in early stage of chronic lymphocytic leukemia correlates with shelterin dysregulation. *Blood* **118:** 1316–1322

Bandyopadhyay D, Curry JL, Lin Q, Richards HW, Chen D, Hornsby PJ, Timchenko NA, Medrano EE (2007) Dynamic assembly of chromatin complexes during cellular senescence: implications for the growth arrest of human melanocytic nevi. *Aging Cell* **6:** 577–591

Bartkova J, Horej Sbreve IZ, Sehested M, Nesland JM, Rajpert-De Meyts E, Skakkebaek NE, Stucki M, Jackson S, Lukas J, Bartek J (2007) DNA damage response mediators MDC1 and 53BP1: constitutive activation and aberrant loss in breast and lung cancer, but not in testicular germ cell tumours. *Oncogene* **26:** 7414–7422

Bartkova J, Horejsi Z, Koed K, Kramer A, Tort F, Zieger K, Guldberg P, Sehested M, Nesland JM, Lukas C, Orntoft T, Lukas J, Bartek J (2005) DNA damage response as a candidate anti-cancer barrier in early human tumorigenesis. *Nature* **434:** 864–870

Bartkova J, Rezaei N, Liontos M, Karakaidos P, Kletsas D, Issaeva N, Vassiliou LV, Kolettas E, Niforou K, Zoumpourlis VC, Takaoka M, Nakagawa H, Tort F, Fugger K, Johansson F, Sehested M, Andersen CL, Dyrskjot L, Orntoft T, Lukas J *et al* (2006) Oncogene-induced senescence is part of the tumorigenesis barrier imposed by DNA damage checkpoints. *Nature* **444:** 633–637

Beliveau A, Bassett E, Lo AT, Garbe J, Rubio MA, Bissell MJ, Campisi J, Yaswen P (2007) p53-dependent integration of telomere and growth factor deprivation signals. *Proc Natl Acad Sci USA* **104:** 4431–4436

Benanti JA, Galloway DA (2004) Normal human fibroblasts are resistant to RAS-induced senescence. *Mol Cell Biol* **24:** 2842–2852

Braig M, Lee S, Loddenkemper C, Rudolph C, Peters AH, Schlegelberger B, Stein H, Dorken B, Jenuwein T, Schmitt CA (2005) Oncogene-induced senescence as an initial barrier in lymphoma development. *Nature* **436:** 660–665

Chen Z, Trotman LC, Shaffer D, Lin HK, Dotan ZA, Niki M, Koutcher JA, Scher HI, Ludwig T, Gerald W, Cordon-Cardo C, Pandolfi PP (2005) Crucial role of p53 dependent cellular senescence in suppression of Pten deficient tumorigenesis. *Nature* **436:** 725–730

Chin K, de Solorzano CO, Knowles D, Jones A, Chou W, Rodriguez EG, Kuo WL, Ljung BM, Chew K, Myambo K, Miranda M, Krig S, Garbe J, Stampfer M, Yaswen P, Gray JW, Lockett SJ (2004) *In situ* analyses of genome instability in breast cancer. *Nat Genet* **36:** 984–988

Chin L, Artandi SE, Shen Q, Tam A, Lee SL, Gottlieb GJ, Greider CW, DePinho RA (1999) p53 deficiency rescues the adverse effects of telomere loss and cooperates with telomere dysfunction to accelerate carcinogenesis. *Cell* **97:** 527–538

Collado M, Gil J, Efeyan A, Guerra C, Schuhmacher AJ, Barradas M, Benguria A, Zaballos A, Flores JM, Barbacid M, Beach D, Serrano M (2005) Tumour biology: senescence in premalignant tumours. *Nature* **436:** 642

Collado M, Serrano M (2010) Senescence in tumours: evidence from mice and humans. *Nat Rev Cancer* **10:** 51–57

Cosme-Blanco W, Shen MF, Lazar AJ, Pathak S, Lozano G, Multani AS, Chang S (2007) Telomere dysfunction suppresses spontaneous tumorigenesis *in vivo* by initiating p53-dependent cellular senescence. *EMBO Rep* **8:** 497–503

Courtois-Cox S, Jones SL, Cichowski K (2008) Many roads lead to oncogene-induced senescence. *Oncogene* **27:** 2801–2809

d'Adda di Fagagna F, Hande MP, Tong WM, Lansdorp PM, Wang ZQ, Jackson SP (1999) Functions of poly(ADP-ribose) polymerase in controlling telomere length and chromosomal stability. *Nat Genet* **23:** 76–80

d'Adda di Fagagna F, Reaper PM, Clay-Farrace L, Fiegler H, Carr P, Von Zglinicki T, Saretzki G, Carter NP, Jackson SP (2003) A DNA damage checkpoint response in telomere-initiated senescence. *Nature* **426:** 194–198

Di Micco R, Fumagalli M, Cicalese A, Piccinin S, Gasparini P, Luise C, Schurra C, Garre M, Nuciforo PG, Bensimon A, Maestro R, Pelicci PG, d'Adda di Fagagna F (2006) Oncogene-induced senescence is a DNA damage response triggered by DNA hyper-replication. *Nature* **444:** 638–642

Di Micco R, Sulli G, Dobreva M, Liontos M, Botrugno OA, Gargiulo G, dal Zuffo R, Matti V, d'Ario G, Montani E, Mercurio C, Hahn WC, Gorgoulis V, Minucci S, d'Adda di Fagagna F (2011) Interplay between oncogene-induced DNA damage response and heterochromatin in senescence and cancer. *Nat Cell Biol* **13:** 292–302

Djojosubroto MW, Chin AC, Go N, Schaetzlein S, Manns MP, Gryaznov S, Harley CB, Rudolph KL (2005) Telomerase antagonists GRN163 and GRN163L inhibit tumor growth and increase chemosensitivity of human hepatoma. *Hepatology* **42:** 1127–1136

Feldser DM, Greider CW (2007) Short telomeres limit tumor progression *in vivo* by inducing senescence. *Cancer Cell* **11:** 461–469

Fumagalli M, Rossiello F, Clerici M, Barozzi S, Cittaro D, Kaplunov JM, Bucci G, Dobreva M, Matti V, Beausejour CM, Herbig U, Longhese MP, d'Adda di Fagagna F (2012) Telomeric DNA damage is irreparable and causes persistent DNA-damage-response activation. *Nat Cell Biol* **14:** 355–365

Gorgoulis VG, Vassiliou LV, Karakaidos P, Zacharatos P, Kotsinas A, Liloglou T, Venere M, Ditullio Jr RA, Kastrinakis NG, Levy B, Kletsas D, Yoneta A, Herlyn M, Kittas C, Halazonetis TD (2005) Activation of the DNA damage checkpoint and genomic instability in human precancerous lesions. *Nature* **434:** 907–913

Gray-Schopfer VC, Cheong SC, Chong H, Chow J, Moss T, Abdel-Malek ZA, Marais R, Wynford-Thomas D, Bennett DC (2006) Cellular senescence in naevi and immortalisation in melanoma: a role for p16? *Br J Cancer* **95:** 496–505

Hahn WC, Counter CM, Lundberg AS, Beijersbergen RL, Brooks MW, Weinberg RA (1999a) Creation of human tumor cells with defined genetic elements. *Nature* **400:** 464–468

Hahn WC, Stewart SA, Brooks MW, York SG, Eaton E, Kurachi A, Beijersbergen RL, Knoll JH, Meyerson M, Weinberg RA (1999b) Inhibition of telomerase limits the growth of human cancer cells. *Nat Med* **5:** 1164–1170

Halazonetis TD, Gorgoulis VG, Bartek J (2008) An oncogene-induced DNA damage model for cancer development. *Science* **319:** 1352–1355

Hanahan D, Weinberg RA (2011) Hallmarks of cancer: the next generation. *Cell* **144:** 646–674

Hande MP, Samper E, Lansdorp P, Blasco MA (1999) Telomere length dynamics and chromosomal instability in cells derived from telomerase null mice. *J Cell Biol* **144:** 589–601

Hao H, Muniz-Medina VM, Mehta H, Thomas NE, Khazak V, Der CJ, Shields JM (2007) Context-dependent roles of mutant B-Raf signaling in melanoma and colorectal carcinoma cell growth. *Mol Cancer Ther* **6:** 2220–2229

Herbig U, Ferreira M, Carey D, Sedivy JM (2006) Cellular senescence in aging primates. *Science* **311:** 1257

Herbig U, Jobling WA, Chen BP, Chen DJ, Sedivy JM (2004) Telomere shortening triggers senescence of human cells through a pathway involving ATM, p53, and p21(CIP1), but Not p16(INK4a). *Mol Cell* **14:** 501–513

Herbig U, Sedivy JM (2006) Regulation of growth arrest in senescence: telomere damage is not the end of the story. *Mech Ageing Dev* **127:** 16–24

Jeyapalan JC, Ferreira M, Sedivy JM, Herbig U (2007) Accumulation of senescent cells in mitotic tissue of aging primates. *Mech Ageing Dev* **128:** 36–44

Kapoor A, Goldberg MS, Cumberland LK, Ratnakumar K, Segura MF, Emanuel PO, Menendez S, Vardabasso C, Leroy G, Vidal CI, Polsky D, Osman I, Garcia BA, Hernando E, Bernstein E (2010) The histone variant macroH2A suppresses melanoma progression through regulation of CDK8. *Nature* **468:** 1105–1109

Kaul Z, Cesare AJ, Huschtscha LI, Neumann AA, Reddel RR (2011) Five dysfunctional telomeres predict onset of senescence in human cells. *EMBO Rep* **13:** 52–59

Kohsaka S, Sasai K, Takahashi K, Akagi T, Tanino M, Kimura T, Nishihara H, Tanaka S (2011) A population of BJ fibroblasts escaped from Ras-induced senescence susceptible to transformation. *Biochem Biophys Res Commun* **410:** 878–884

Lansdorp PM (2005) Major cutbacks at chromosome ends. *Trends Biochem Sci* **30:** 388–395

Lebofsky R, Bensimon A (2003) Single DNA molecule analysis: applications of molecular combing. *Brief Funct Genomic Proteomic* **1:** 385–396

Lee AC, Fenster BE, Ito H, Takeda K, Bae NS, Hirai T, Yu ZX, Ferrans VJ, Howard BH, Finkel T (1999) Ras proteins induce senescence by altering the intracellular levels of reactive oxygen species. *J Biol Chem* **274:** 7936–7940

Majumder PK, Grisanzio C, O'Connell F, Barry M, Brito JM, Xu Q, Guney I, Berger R, Herman P, Bikoff R, Fedele G, Baek WK, Wang S, Ellwood-Yen K, Wu H, Sawyers CL, Signoretti S, Hahn WC, Loda M, Sellers WR (2008) A prostatic intraepithelial neoplasia-dependent p27 Kip1 checkpoint induces senescence and inhibits cell proliferation and cancer progression. *Cancer Cell* **14:** 146–155

Martinez P, Thanasoula M, Munoz P, Liao C, Tejera A, McNees C, Flores JM, Fernandez-Capetillo O, Tarsounas M, Blasco MA (2009) Increased telomere fragility and fusions resulting from TRF1 deficiency lead to degenerative pathologies and increased cancer in mice. *Genes Dev* **23:** 2060–2075

Meeker AK, Hicks JL, Gabrielson E, Strauss WM, De Marzo AM, Argani P (2004a) Telomere shortening occurs in subsets of normal breast epithelium as well as *in situ* and invasive carcinoma. *Am J Pathol* **164:** 925–935

Meeker AK, Hicks JL, Iacobuzio-Donahue CA, Montgomery EA, Westra WH, Chan TY, Ronnett BM, De Marzo AM (2004b) Telomere length abnormalities occur early in the initiation of epithelial carcinogenesis. *Clin Cancer Res* **10:** 3317–3326

Michaloglou C, Vredeveld LC, Mooi WJ, Peeper DS (2008) BRAF(E600) in benign and malignant human tumours. *Oncogene* **27:** 877–895

Michaloglou C, Vredeveld LCW, Soengas MS, Denoyelle C, Kuilman T, van der Horst CMAM, Majoor DM, Shay JW, Mooi WJ, Peeper DS (2005) $BRAF^{E600}$ associated senescence like cell cycle arrest of human naevi. *Nature* **436:** 720–724

Morgenstern JP, Land H (1990) Advanced mammalian gene transfer: high titre retroviral vectors with multiple drug selection markers and a complementary helper-free packaging cell line. *Nucleic Acids Res* **18:** 3587–3596

Nuciforo PG, Luise C, Capra M, Pelosi G, d'Adda di Fagagna F (2007) Complex engagement of DNA damage response pathways in human cancer and in lung tumor progression. *Carcinogenesis* **28:** 2082–2088

Poonepalli A, Balakrishnan L, Khaw AK, Low GK, Jayapal M, Bhattacharjee RN, Akira S, Balajee AS, Hande MP (2005) Lack of poly(ADP-ribose) polymerase-1 gene product enhances cellular sensitivity to arsenite. *Cancer Res* **65:** 10977–10983

Qi L, Strong MA, Karim BO, Armanios M, Huso DL, Greider CW (2003) Short telomeres and ataxia-telangiectasia mutated deficiency cooperatively increase telomere dysfunction and suppress tumorigenesis. *Cancer Res* **63:** 8188–8196

Robinson K, Asawachaicharn N, Galloway DA, Grandori C (2009) c-Myc accelerates S-phase and requires WRN to avoid replication stress. *PLoS One* **4:** e5951

Rudolph KL, Millard M, Bosenberg MW, DePinho RA (2001) Telomere dysfunction and evolution of intestinal carcinoma in mice and humans. *Nat Genet* **28:** 155–159

Sarkisian CJ, Keister BA, Stairs DB, Boxer RB, Moody SE, Chodosh LA (2007) Dose-dependent oncogene-induced senescence *in vivo* and its evasion during mammary tumorigenesis. *Nat Cell Biol* **9:** 493–505

Schultz LB, Chehab NH, Malikzay A, Halazonetis TD (2000) p53 binding protein 1 (53BP1) is an early participant in the cellular response to DNA double-strand breaks. *J Cell Biol* **151:** 1381–1390

Sfeir A, Kosiyatrakul ST, Hockemeyer D, MacRae SL, Karlseder J, Schildkraut CL, de Lange T (2009) Mammalian telomeres resemble fragile sites and require TRF1 for efficient replication. *Cell* **138:** 90–103

Sharpless NE, DePinho RA (2005) Cancer: crime and punishment. *Nature* **436:** 636–637

Sherman MY, Meng L, Stampfer M, Gabai VL, Yaglom JA (2011) Oncogenes induce senescence with incomplete growth arrest and suppress the DNA damage response in immortalized cells. *Aging Cell* **10:** 949–961

Sun B, Chen M, Hawks CL, Pereira-Smith OM, Hornsby PJ (2005) The minimal set of genetic alterations required for conversion of primary human fibroblasts to cancer cells in the subrenal capsule assay. *Neoplasia* **7:** 585–593

Takai H, Smogorzewska A, de Lange T (2003) DNA damage foci at dysfunctional telomeres. *Curr Biol* **13:** 1549–1556

Tuveson DA, Shaw AT, Willis NA, Silver DP, Jackson EL, Chang S, Mercer KL, Grochow R, Hock H, Crowley D, Hingorani SR, Zaks T, King C, Jacobetz MA, Wang L, Bronson RT, Orkin SH, DePinho RA, Jacks T (2004) Endogenous oncogenic K-ras(G12D) stimulates proliferation and widespread neoplastic and developmental defects. *Cancer Cell* **5:** 375–387

Wei S, Wei W, Sedivy JM (1999) Expression of catalytically active telomerase does not prevent premature senescence caused by overexpression of oncogenic Ha-Ras in normal human fibroblasts. *Cancer Res* **59:** 1539–1543

Wong KK, Maser RS, Bachoo RM, Menon J, Carrasco DR, Gu Y, Alt FW, DePinho RA (2003) Telomere dysfunction and Atm deficiency compromises organ homeostasis and accelerates ageing. *Nature* **421:** 643–648

Wong VC, Ma J, Hawkins CE (2009) Telomerase inhibition induces acute ATM-dependent growth arrest in human astrocytomas. *Cancer Lett* **274:** 151–159

Ye J, Lenain C, Bauwens S, Rizzo A, Saint-Leger A, Poulet A, Benarroch D, Magdinier F, Morere J, Amiard S, Verhoeyen E, Britton S, Calsou P, Salles B, Bizard A, Nadal M, Salvati E, Sabatier L, Wu Y, Biroccio A *et al* (2010) TRF2 and apollo cooperate with topoisomerase 2alpha to protect human telomeres from replicative damage. *Cell* **142:** 230–242

Zhang R, Chen W, Adams PD (2007) Molecular dissection of formation of senescence-associated heterochromatin foci. *Mol Cell Biol* **27:** 2343–2358

Zhang R, Poustovoitov MV, Ye X, Santos HA, Chen W, Daganzo SM, Erzberger JP, Serebriiskii IG, Canutescu AA, Dunbrack RL, Pehrson JR, Berger JM, Kaufman PD, Adams PD (2005) Formation of MacroH2A-containing senescence-associated heterochromatin foci and senescence driven by ASF1a and HIRA. *Dev Cell* **8:** 19–30